Circular RNAs arising from synaptic host genes are modulated by SFPQ RNA-binding protein and increased during human neuronal differentiation

Michelle Watts[1,2], Marika Oksanen[1,2,3], Sanna Lejerkrans[1,2], Francesca Mastropasqua[1,2], Myriam Gorospe[3] and Kristiina Tammimies[1,2,*]

[1]Center of Neurodevelopmental Disorders (KIND), Centre for Psychiatry Research, Department of Women's and Children's Health, Karolinska Institutet and Stockholm Health Care Services, Region Stockholm, Stockholm, Sweden.
[2]Astrid Lindgren Children's Hospital, Karolinska University Hospital, Region Stockholm, Stockholm, Sweden.
[3]Laboratory of Genetics and Genomics, National Institute on Aging Intramural Research Program, NIH, Baltimore, MD, USA.

[*]Correspondence:
Kristiina Tammimies, PhD
E-mail: kristiina.tammimies@ki.se
Postal address: BioClinicum J9:30, Visionsgatan 4, 171 56 Solna, Sweden

Abstract

Circular RNAs (circRNAs) are emerging as a key component of the complex neural transcriptome implicated in brain development. However, the specific expression patterns and functions of circRNAs in human neuronal differentiation have not been explored. Using total RNA sequencing analysis, we identified expressed circRNAs during the differentiation of human neuroepithelial stem (NES) cells into developing neurons and discovered that many circRNAs originated from host genes with synaptic functions. Interestingly, when assessing population data and rare *de novo* variants in autism spectrum disorder (ASD) candidate host genes, exons giving rise to circRNAs had a significantly higher frequency of genetic variants. Screening for RNA-binding protein sites identified enrichment of Splicing Factor Proline and Glutamine Rich (SFPQ) motifs in increased circRNAs, several of which we validated as being reduced by SFPQ knockdown and enriched in SFPQ ribonucleoprotein complexes. Our study provides an in-depth characterisation of circRNAs in a human neuronal differentiation model and highlights SFPQ as both a regulator and binding partner of circRNAs elevated during neuronal maturation.

Introduction

CircRNAs represent a unique class of RNA molecules formed following non-canonical back-splicing of exon-exon junctions (Cocquerelle *et al*, 1992; Nigro *et al*, 1991). These covalently closed, circularised RNAs lack 5'cap and 3'poly-A structures resulting in highly stable molecules, resistant to enzymatic degradation (Jeck *et al*, 2013; Memczak *et al*, 2013). Since their initial discovery, the circRNA transcriptome has expanded rapidly with the advent of sequencing approaches and bioinformatic tools designed to detect back-spliced junctions in RNA-sequencing (RNAseq) data (Memczak *et al.*, 2013; Salzman *et al*, 2013; Salzman *et al*, 2012). Although once thought to be non-functional by-products of spurious splicing events, numerous functional roles of circRNAs have now been identified, including microRNA (miRNA) sponging (Memczak *et al.*, 2013), transcriptional regulation (Conn *et al*, 2017; Pandey *et al*, 2020), RNA-binding protein function (Panda *et al*, 2017; Tsitsipatis *et al*, 2021), and modulation of protein interactions (Barbagallo *et al*, 2019; Du *et al*, 2016). These roles highlight the vast diversity of possible functions for circRNAs, most of which are unknown.

As is often observed for mechanisms such as microRNAs or splicing factors that diversify the mammalian transcriptome, circRNA species are highly enriched in the nervous system (Memczak *et al.*, 2013; Rybak-Wolf *et al*, 2015; You *et al*, 2015). Spatio-temporal regulation of circRNA expression within the brain is also dynamic, differing across brain regions and developmental stages (Chen *et al*, 2019; Veno *et al*, 2015; You *et al.*, 2015). Brain and neuronal expressed circRNAs have also been

found to arise from host genes with synaptic functions and display specific enrichment within synaptosomes as well as regulation in response to neuronal activation (Gokool *et al*, 2020; You *et al.*, 2015). Under various circumstances, this regulation appears independent of corresponding host genes and, in some cases, circRNA levels far exceed linear host RNA levels (Rybak-Wolf *et al.*, 2015; You *et al.*, 2015), underscoring the importance of precise modulation of circRNAs during neuronal development.

Accumulating evidence suggests that circRNAs are not only important for neuronal function but also for brain development. Differential expression of circRNAs has been found to occur during neuronal differentiation, both in mice and in cell culture models such as the human neuroblastoma cell line SH-SY5Y, with several specific circRNAs were found to have a regulatory role in this process (Hollensen *et al*, 2020; Li *et al*, 2022b; Suenkel *et al*, 2020; Yang *et al*, 2019; Yang *et al*, 2018). Additionally, a number of circRNAs have been identified as being dysregulated in Autism Spectrum Disorder (ASD) (Chen *et al*, 2020; Gokool *et al.*, 2020), while a depletion of circRNAs has been observed in individuals with Schizophrenia (SCZ) (Mahmoudi *et al*, 2019). Currently, however, our understanding of circRNA regulation and function in human neurodevelopment remains largely unexplored.

While evaluation of circRNAs in the human brain is limited to post-mortem analyses, derivation of mature neurons from human induced pluripotent stem cells (hiPSCs) allows for modelling of neuronal differentiation in a human genetic background (Dolmetsch & Geschwind, 2011). Computational methods to detect back-spliced junctions in total RNAseq data also allow for the discovery of circRNAs without the need for specialised treatment of RNA samples as well as comparison with gene expression from the same data (Hansen, 2018). We combined these methodologies to examine the circRNA landscape of hiPSC-derived neuroepithelial stem (NES) cells and developing neurons, revealing an increase in circRNAs during differentiation, arising from host genes with synaptic functions. CircRNA-forming exons were also found to harbour genetic variants at a higher rate, including rare *de novo* ASD-associated variants, in comparison to exons from the same host gene that were not circularized. In addition, we investigated the potential functionality of elevated circRNAs and identified an enrichment of binding motifs for Splicing Factor Proline and Glutamine Rich (SFPQ). Predicted circRNA targets of SFPQ were found to be depleted during neuronal differentiation following SFPQ knockdown including a novel circRNA from the Regulating Synaptic Membrane Exocytosis 1 (RIMS1) host gene that was specifically enriched by SFPQ immunoprecipitation above its corresponding linear isoform.

Results

Detection of robust circRNA production during NES differentiation from total RNAseq data

To analyse circRNAs in human neuronal differentiation, hiPSC-derived NES cells were differentiated as previously described (Becker *et al*, 2020). Total RNA was collected and sequenced from cells in their proliferative, neural progenitor state (NES) and two time points of differentiation. First, at day five (D5), when a neural identity has been adopted and neurite outgrowth/axon specification is underway, and second at day 28 (D28), when extensive neural networks, but not yet mature active connections, have been established **[Fig 1a]**. To reduce spurious circRNA discovery, three detection programs (CIRCexplorer2, CIRI, MapSplice) with reported low false positive rates were utilised (Hansen, 2018). A total of 60,531 detected circRNAs were filtered for minimum expression, leaving 6,540 circRNAs (~10.8%) for downstream analysis. These were further filtered to include only circRNAs detected by at least two programs, which represented the majority of the expression filtered dataset (6,385; ~97.6%) **[Fig 1b]**. Among these, 66% were known circRNAs reported in circBase (Glazar *et al*, 2014), 34% were novel circRNAs (not yet reported in circBase), and 8.5% of the dataset were '*de novo'* circRNAs that did not annotate to known splice sites. The entire filtered dataset of 6,385 circRNAs was derived from 2,743 unique host genes, with 1,377 genes producing two or more circRNA isoforms and 50 'hotspot' genes that generated over ten circRNAs **[Table S1a]**. All circRNAs analysed and reported in Table S1 have been assigned an ID based on host gene name and back-spliced junction genomic locations. Where available, corresponding circBase IDs are provided. For simplicity, specific circRNAs referenced within this text are referred to only by host gene name with alphabetical indexing for referencing circRNA isoforms.

Differentially expressed circRNAs (DEcircs) in NES differentiation were detected using DESeq2 with log fold-change shrinkage estimation (lfc-shrink) for increased stringency. We observed a predominant increase of circRNA expression with pairwise comparisons finding 33 circRNAs up and 8 circRNAs down at D5 compared to NES and 660 circRNAs up and 95 down at D28 compared to NES (p-adjusted <0.05, lfc-shrink ≥|2|) **[Fig 1c; Table S1b-d]**. Almost all circRNAs (32/33) whose expression was increased at the early differentiation time point (D5) also remained significantly increased at D28 **[Fig 1d]**. Clustering results using the likelihood ratio test, which incorporates all time points, similarly highlighted a primary cluster of circRNAs with a pattern of increasing abundance throughout differentiation **[Fig 1e; Table S1e,f]**.

To validate whether detected circRNAs occurred endogenously and are differentially expressed during differentiation, we selected 20 significant DEcircs and designed divergent primer pairs to selectively amplify back-spliced junctions **[Fig S1a]**. PCR amplification and gel

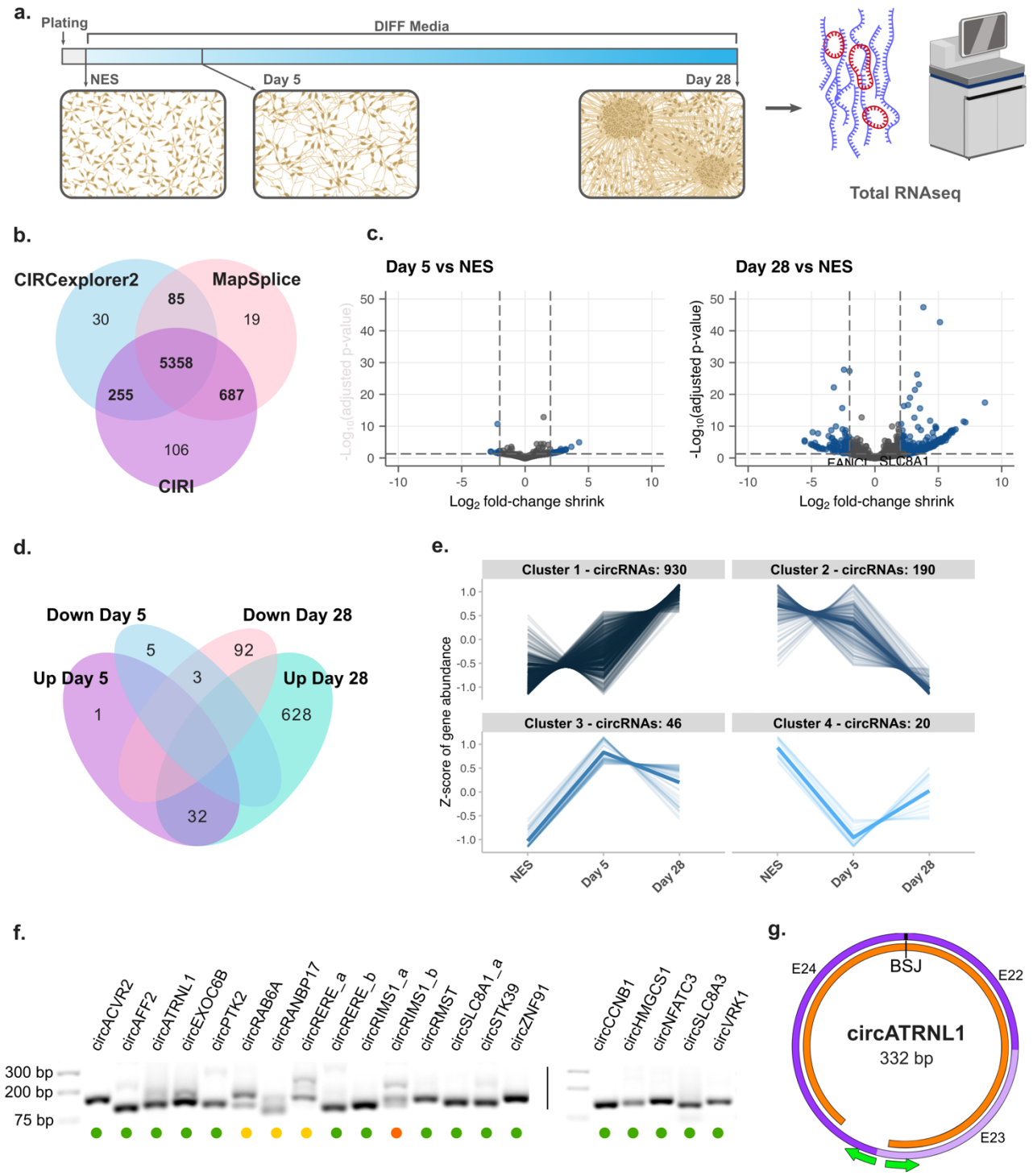

Figure 1. Detection and validation of circRNAs in human neuronal differentiation**. a.** Schematic representation of sample and data collection. **b.** Venn diagram of circRNAs detected from three different circRNA detection programs, numbers highlighted in bold indicated circRNAs included in downstream analysis. **c.** Volcano plots of differentially expressed circRNAs at D5 and D28 of differentiation compared to NES. **d.** Venn diagram of significantly dysregulated circRNAs (padj < 0.05 and lfc-shrink ≥|2|). **e.** Cluster analysis of circRNAs differentially expressed throughout differentiation. **f.** Detection of top differentially

expressed circRNAs by PCR with divergent junction primers. Green = single, expected band, yellow = predominant expected band with additional spurious band/s, orange = expected band not detected. **g.** Example schematic of sanger sequencing validation of circRNA exon retention in *circATRNL1*. Exons are shown in purple, green arrows indicate primer location, and sequencing alignment is shown in orange.

electrophoresis found a clear, predominant band of the expected size for 16/20 primer pairs, three primer pairs also amplified other products in addition to the major product of expected size, while one primer pair, *circRIMS1_b*, was unsuccessful in producing a band of expected size **[Fig 1f]**. While spurious bands may arise from mispriming, they may also originate from multimeric cDNA templates produced by rolling-circle amplification of alternate circRNA isoforms (Das et al, 2019), particularly for *circRIMS1_b* as this host gene is known to produce numerous circRNA isoforms (Rahimi et al, 2021). Using quantitative PCR (qPCR) analysis of replicate samples, similar differential expression of circRNAs was also observed at D28 when compared to NES, particularly for increased circRNAs **[Fig S1b]** and qPCR log fold-changes strongly correlated with RNAseq lfc-shrink values ($R = 0.8$, $p = 1.2e-4$). Finally, secondary divergent primer pairs were designed to confirm circRNA annotation and determine internal exon structure in circRNAs with non-consecutive back-spliced exons **[Fig S1c]**. Among primer pairs which amplified enough product, all except *circRIMS1_a*, produced a single band. Sanger sequencing confirmed back-spliced exon identity in all circRNAs as well as internal exon retention, where relevant **[Fig 1g and Fig S2]**. A second larger product of the primer pair for *circRIMS1_a* (*circRIMS1_a2*) was found to contain an additional 88-b sequence which maps to an intronic region between, but not adjacent to, exons 7 and 8 (GRCh37-chr6:72299090-72299177) which is likely to be an as-yet unannotated exon of RIMS1. Finally, as an additional validation, the dataset was compared with circRNAs detected by Gokool *et al*, which represents the largest dataset of human brain circRNAs (197 post-mortem samples), and ~80% of circRNAs in our study were found to be represented. Taken together, these results indicate that our pipeline for circRNA detection from total RNAseq data was successful in identifying genuine circRNAs that are differentially expressed during neuronal differentiation.

CircRNAs increased during NES differentiation arise from synaptic host genes

Given that NES differentiation primarily caused an increase of circRNA expression, functional annotations associated with host genes of this circRNA subset were examined. Gene ontology terms related to synaptic processes, ion transport, and neuron development were found to be most highly enriched among Cluster 1 circRNAs as well as in positive gene set enrichment analysis (GSEA) of D28 vs NES DEcircs **[Fig 2a,b and Table S2]**. While similar pathways were identified as positively

144 enriched from GSEA of D5 vs NES, only one reached significance (GO:0051962-Positive regulation
145 of nervous system development*;* p-adjusted <0.05). Of interest, GSEA of D28 vs D5 found only cell-
146 cell adhesion as an enriched process, while multiple processes related to early neuronal specification,
147 such as cell projection and axonogenesis, were negatively enriched **[Fig S3a]**. We also examined the
148 enrichment of neurodevelopmental disorder (NDD) risk genes since circRNA expression has
149 previously been found to be disrupted in individuals with ASD and SCZ. The tested genes included
150 ASD genes from the Simons Foundation Autism Research Initiative (SFARI) database, collated SCZ
151 risk genes **[Table S3]**, and developmental disorder-related genes covering broader phenotypes (Li *et*
152 *al*, 2022a). We found significant enrichment of ASD genes among circRNAs increased at D28 vs NES,
153 and significant enrichment of SCZ risk genes in Cluster 4 circRNAs **[Fig S3b,c]**.

154 Employing the same RNAseq dataset, we performed a differential expression analysis of linear
155 RNAs to identify regulatory patterns and gene ontology terms. The expression of linear RNAs was
156 found to follow a similar regulatory pattern to that of circRNAs, with a higher proportion of linear RNAs
157 increased at D28 vs NES (2,904 genes compared to 1,363 decreased; p-adjusted <0.05, lfc-shrink
158 ≥|2|) **[Fig S3d and Table S4a]**. GSEA also revealed enrichment of similar pathways related to
159 synaptic function among linear RNAs increased by differentiation **[Fig S3e and Table S4b]**. Since
160 multiple studies have found discordances between the changes in circRNA levels and the changes in
161 the levels of linear RNAs from the same host gene, we compared changes in circRNA and linear
162 counterparts. As shown, a moderate but significant positive correlation was detected ($R = 0.5$, $p < 2.2e-$
163 16). Plotting of lfc-shrink correlates highlighted this same positive linear association; however, there
164 was an evident shift from the linear distribution suggesting that highly increased circRNAs had higher
165 fold-changes than their linear counterparts [**Fig 2c]**. A direct comparison of circRNAs to linear RNA
166 counterparts found this same trend among the top 20 circRNAs with an average increase of circRNA
167 expression of ~6.7 fold higher than linear RNAs **[Fig S4]**. Additionally, among circRNAs increased at
168 D28 vs NES, a large majority (71.6%) were over two-fold higher than the linear counterparts from the
169 same host genes, supporting a non-linear relationship between the expression of these two RNA
170 forms.

171 To further explore the relationship between linear RNA and circRNA regulation, we analysed
172 differential exon usage in our dataset using DEXseq. All exon bins detected by DEXseq were analysed
173 as exons, including those corresponding to circRNA-forming exons. Comparing cells differentiated to
174 D28 with NES cells we identified a large number of differentially used exons (19,502 exons; p-adjusted
175 <0.05, lfc ≥|2|). Among these, the number of exons with eleveated expression was over three times
176 higher than exons with reduced expression (4,680 down:14,822 up), implying substantially increased
177 exon inclusion at D28. This corresponds with alternative splicing of 4,904 RNAs with an average of

178 ~31 exons. When enrichment of gene ontology terms among alternatively spliced RNAs were
179 examined, pathways related to the ribosome and spliceosome were most significantly enriched **[Fig**
180 **S3f]**.

181 To establish if alternative splicing is associated with circRNA biogenesis and/or increased
182 abundance of circRNAs at D28, the rate of alternate splicing (based on differential exon usage at D28
183 vs. NES) was compared among three groups: all linear RNAs, linear RNAs sharing host RNAs with
184 circRNAs, and linear RNAs sharing host RNAs with circRNAs increased at D28. While alternative
185 splicing was ~3-fold higher among RNAs which host circRNAs ($p < 0.0001$) compared to all RNAs,
186 there was no difference in alternate splicing rate between all host RNAs and hosts of circRNAs

187

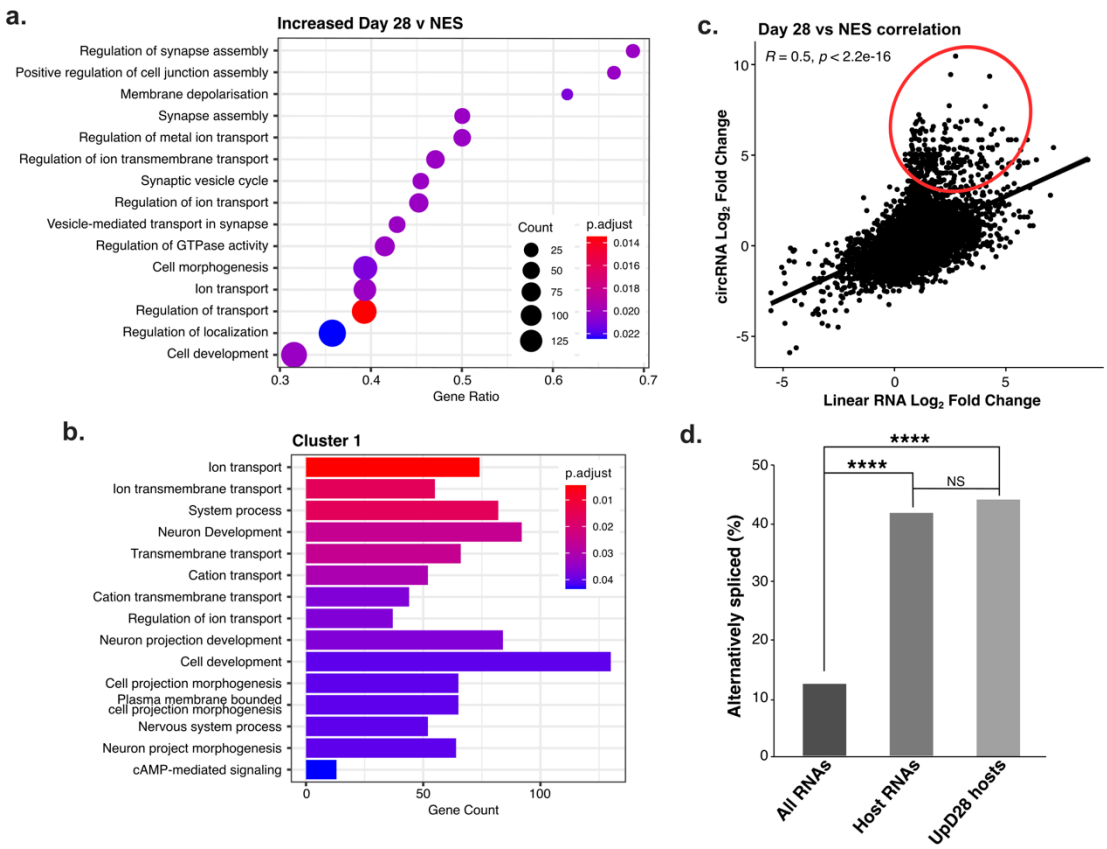

188

189

190 **Figure 2.** CircRNAs increased during NES differentiation arise from host genes with synaptic function. **a.**
191 GSEA of gene ontology – biological process terms among the genes that host circRNAs increased at D28
192 of differentiation compared to NES. **b.** Most highly enriched gene ontology – biological process terms
193 among host genes of Cluster 1 circRNAs. **c.** Correlation of log fold-changes for circRNAs and their
194 corresponding linear counterparts. **d.** Alternative splicing comparison between all RNAs, RNA which host
195 circRNAs and RNAs that host circRNAs increased at D28 vs. NES. **** = $p < 0.0001$, hypergeometric p-
196 value test.

197 increased at D28 (p = 0.153) **[Fig 2d]**. Similarly, we found no correlation between circRNA fold-
198 changes and estimated exon fold-changes (R = -0.018), suggesting that increased abundance of
199 circRNAs during NES differentiation is independent of general splicing of host precursor RNAs.
200
201

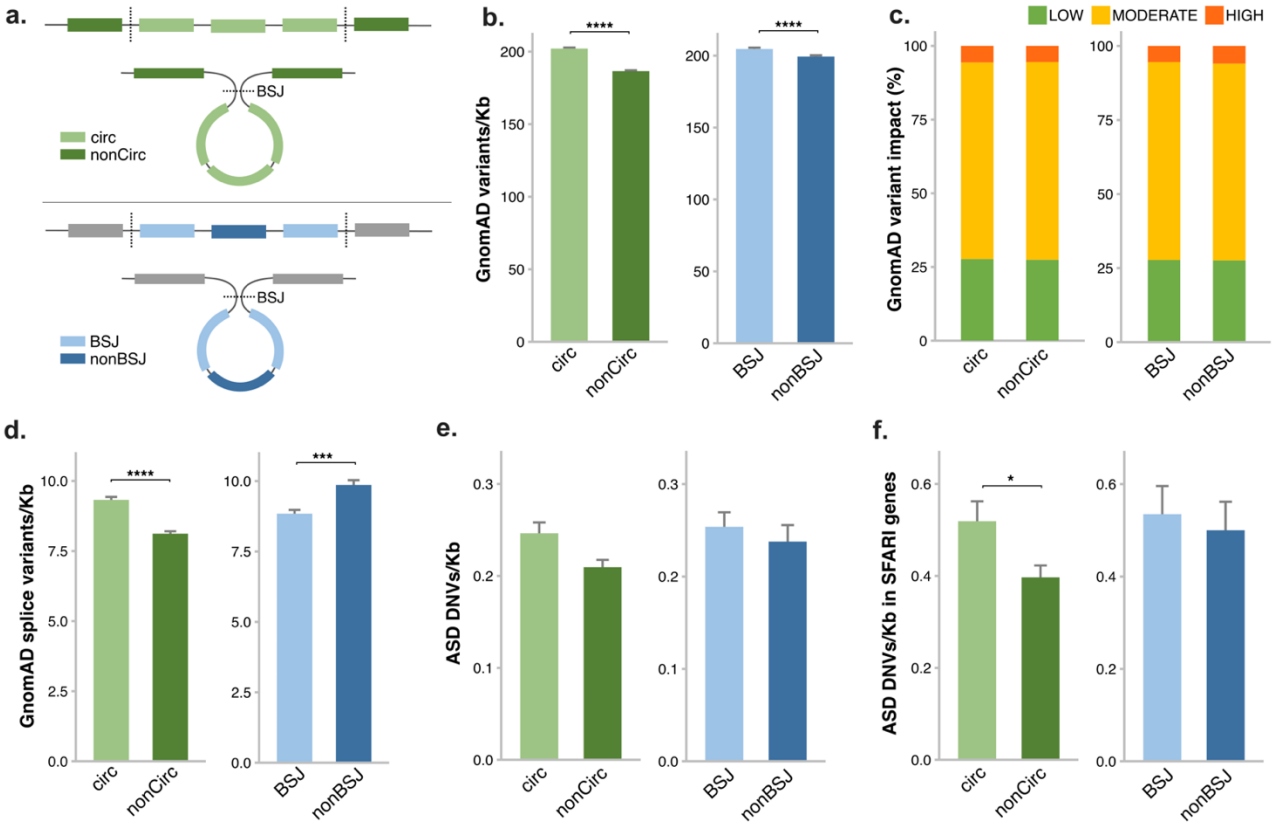

202
203

204 **Figure 3.** Genetic variant frequency in circRNA-forming exons**. A.** Schematic depicting how exons were
205 subdivided for comparative analysis. BSJ = back-spliced junctions. **B.** Frequency of GnomAD exon
206 variants for circRNAs detected in this study, normalised for exon size (Kb). **C.** Proportion of GnomAD exon
207 variants annotated as having either low, medium, or high impact. **D.** Frequency of GnomAD splice-region
208 exon variants/Kb. **E.** Frequency of rare *de novo* ASD variants/Kb. **F.** Frequency of rare *de novo* ASD
209 variants/Kb in exons of circRNAs arising from ASD-associated SFARI host genes. Two sample Z-
210 test/Wilcox test, **** = $p < 0.0001$, *** = $p < 0.001$ * = $p < 0.05$. DNVs = *de novo* variants.

211

212 *Variant frequency is increased in circRNA-forming exons*

213 To further assess the role of circRNAs in human health and disorders, we examined genetic variant
214 burden in circRNA-forming exons. Exons were classified into circ and nonCirc groups based on all
215 exons of the longest annotated transcript containing the back-spliced exon(s). CircRNA exons were

216 further differentiated as exons that either form BSJs or do not form BSJs (nonBSJ exons) **[Fig 3a]**.
217 Genetic variants included in the Genome Aggregation Database (gnomAD) were initially utilised to
218 examine the frequency of circRNA exon variation in the general population. Rates of genetic variation
219 were found to be slightly higher in both circ ($p = 2.2e-16$) and BSJ ($p = 1.4e-5$) exons when compared
220 with nonCirc and nonBSJ exons, respectively **[Fig 3b]**. However, no shift was observed in the
221 annotation of variant impact among exon groups **[Fig 3c]** or in the proportion of missense variants or
222 the proportion of missense variants identified as deleterious **[Fig S5a,b]**. When we limited the analysis
223 to splice variants, a higher rate among circRNA-forming exons in comparison to nonCirc exons was
224 detected ($p < 2.2e-16$). Furthermore, among circRNA-forming exons, the rate of splice variants was
225 significantly lower in BSJ exons compared with nonBSJ exons ($p = 1.1e-4$) **[Fig 3d]**. These
226 observations suggest circRNA-forming and BSJ exons are subject to increased variation while
227 splicing variants are less frequent among back-spliced exons.

228 Next, we examined the frequency of rare *de novo* variants found in ASD from a large exome
229 sequencing study from 21,219 family-based samples, including 12,166 variants in 6,430 individuals
230 with ASD (Satterstrom *et al*, 2020). We identified similar results as for gnomAD variants in that *de*
231 *novo* ASD variants occurred at a slightly higher rate in circ and BSJ exons **[Fig 3e]**. This increase in
232 circ exon variants was significant specifically when examining circRNAs formed from ASD-associated
233 SFARI host genes ($p = 0.0384$) **[Fig 3f]**. Among circ exons, 72 ASD variants were found to occur
234 within host genes for circRNAs increased by differentiation (86 exons from 64 genes). Of these, the
235 majority (56/64) had only one circ exon variant while eight genes carried two, including genes from
236 SFARI, namely *HECTD4, MYT1L*, *NRXN1* and *RAB2A*. An additional 3,633 rare *de novo* variants in
237 2,179 unaffected sibling controls from the same cohort were also examined for frequency in circRNA
238 exons. No significant differences in variant frequency were observed across exon groups, although a
239 trend for increased variants in BSJ above non-BSJ exons was detected ($p = 0.06017$) **[Fig S5c,d]**.

240 Due to a lack of a comparable large resource for SCZ, we collated SCZ variants reported from
241 several sources **[Table S5]**. In total, 2,035 rare *de novo* variants identified in individuals diagnosed
242 with either Schizophrenia or schizoaffective disorder were included. When comparing the frequency
243 of SCZ variants, we found no differences across exon groups either among all transcripts or when
244 comparing variants specifically in SCZ risk genes **[Fig S5e,f]**. However, within host genes of circRNAs
245 increased by differentiation, 15 SCZ variants were identified (15 exons from 14 genes), three of which
246 are SCZ risk genes (*RERE*, *EPHB2* and *MAN2A1*).

247

248 *Binding site enrichment in circRNAs differentially expressed during NES differentiation*

249 Given that circRNA functionality remains largely unknown, differentially expressed circRNAs were
250 screened *en masse* for potential function by searching for binding sites among circRNA sequences.
251 The discovery that the highly abundant circRNA, *CDR1as,* functions in sequestering miR-7 through
252 numerous seed sites (Memczak *et al.*, 2013; Piwecka *et al*, 2017) has since led to frequent reporting
253 of predicted circRNA:miRNA:mRNA interactions (Chen *et al.*, 2020; Dell'Orco *et al*, 2021; Liu *et al*,
254 2021; Ma *et al*, 2019). We, therefore, first investigated miRNA sponging by exploring possible
255 interactions between miRNAs and DEcircs. We limited our search to 125 human miRNAs previously
256 associated with neurodevelopment or NDDs, which were most of interest to our study **[Table S6a,b]**.
257 To construct putative circRNA:miRNA:mRNA interaction axes, binding sites for these miRNAs were
258 predicted in both DEcircs as well as 3'UTRs of differentially expressed RNAs **[Table S6c,d]**. Based
259 on canonical miRNA regulation where miRNAs repress gene expression and circRNA sponges
260 alleviate target repression, circRNAs with predicted miRNA binding sites were matched to mRNAs
261 containing binding sites for the same miRNA and with the same pattern of regulation. We found no
262 circRNAs to have a high number of binding sites for any particular miRNA, with a maximum of three
263 sites identified in any single circRNA. This is consistent with other reports that enrichment of miR-7
264 sites in CDR1as is a unique phenomenon among circRNAs (Guo *et al*, 2014; You *et al.*, 2015).
265 Therefore, while we report identified circRNA:miRNA:mRNA interactions in **Table S6e,** we do not
266 expect that these circRNAs function in miR-sponging.

267 Next, we examined the enrichment of RNA-binding protein (RBP) motifs among DEcirc
268 sequences. A number of motifs were found to be enriched among different subsets of DEcircs,
269 including two motifs enriched among increased circRNAs **[Table S7a]**. These two motifs were
270 associated with two splicing factor RBPs, namely, TIA1 Cytotoxic Granule Associated RNA Binding
271 Protein Like 1 (TIAL1) and Splicing Factor Proline and Glutamine Rich (SFPQ) **[Fig 4a,b]**. These
272 results highlighted a possible functional link between TIAL1 and SFPQ RBPs and the increased
273 abundance of circRNAs in neuronal differentiation.

274

275 *SFPQ regulates expression of circRNAs in NES differentiation*

276 To further test the relationship between increased circRNAs and enriched RBP motifs, expression of
277 SFPQ and TIAL1 mRNA in NES differentiation was first established. Normalised counts from RNAseq
278 analysis indicated that both RBPs were expressed at all time points albeit both with reduced
279 expression at D28 and with SFPQ levels around tenfold higher than TIAL1 **[Fig 4c,d]**. From motif
280 analysis of circRNA sequences, a number of 'top' putative targets for SFPQ and TIAL1 were
281 subsequently chosen based on motif frequency, base mean expression and log fold-change values

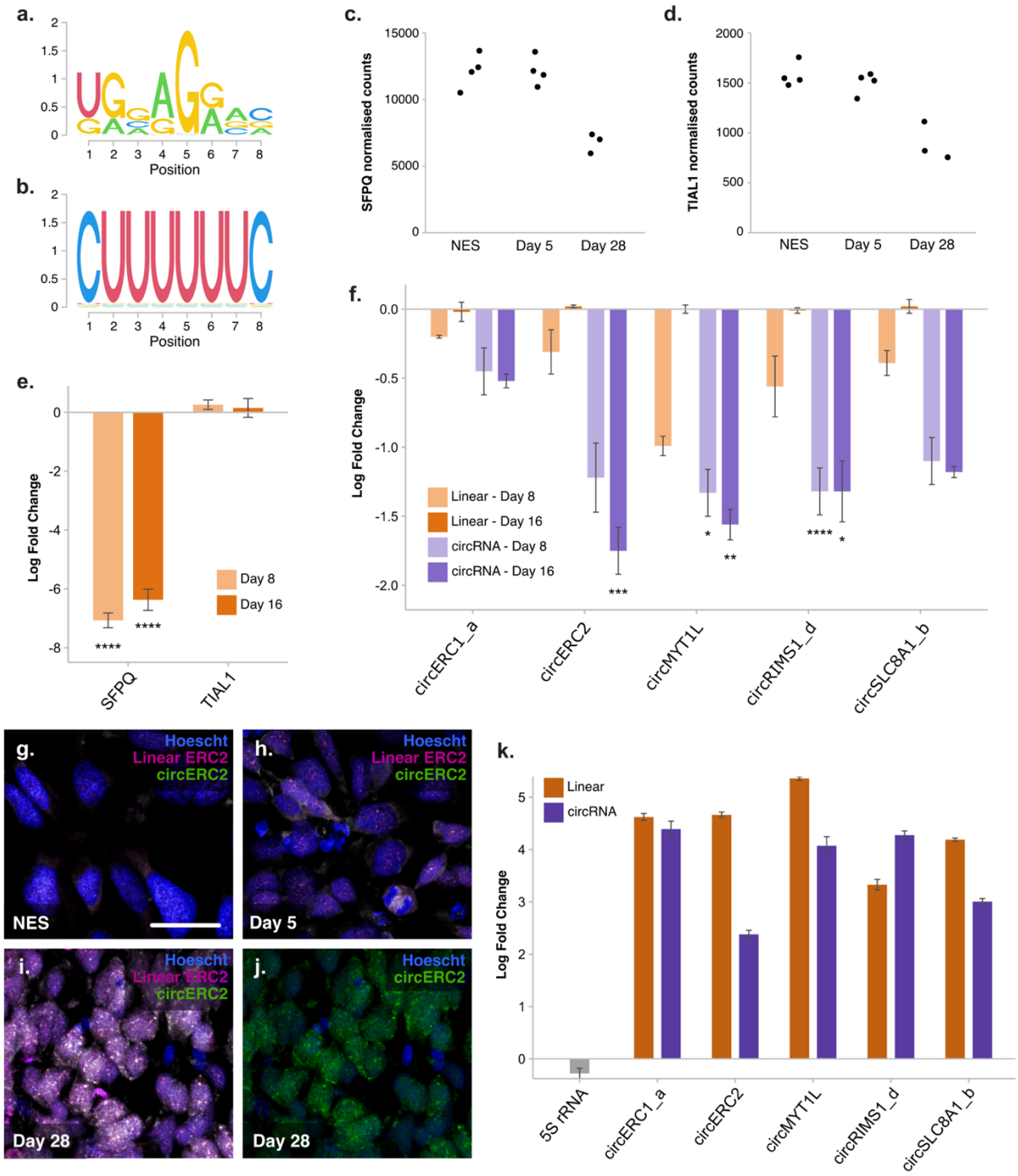

Figure 4. RNA-binding protein SFPQ regulates and binds to subsets of circRNAs during neuronal differentiation**. a.** SFPQ motif enriched among circRNAs increased at D28 v D5. **b.** TIAL1 motif enriched among circRNAs increased at D28 v NES. **c.** Normalised counts of SFPQ RNA during NES differentiation. **d.** Normalised counts of SFPQ RNA during NES differentiation. **e.** Detection of SFPQ and TIAL1 mRNA following siRNA treatment (n = 3). **f.** Relative expression of SFPQ targets following SFPQ knockdown (n = 3)**. g-j.** *In situ* detection of *circERC2* and its linear isoform in undifferentiated NES cells (**g**), and cells at D5 (**h**) and D28 (**i,j**) of differentiation. Blue = Hoechst nuclear counter stain, magenta = linear ERC2 probe,

green = *circERC2* probe. Scale bar in g = 25 µm, applies to g-j. images are representative of staining from biological replicates (*n* = 3). **k.** SFPQ RIP followed by RT-qPCR analysis to identify SFPQ targets and *5S* rRNA control, normalised to IgG RIP samples from D28 differentiated neurons (*n* = 2). **** = $p < 0.0001$, *** = $p < 0.001$, ** = $p < 0.01$, * = $p < 0.05$, one-way ANOVA, Tukey post-hoc analysis, Bonferroni adjusted. Error bars represent standard error.

[Table S7b,c]. Elevated expression of all selected circRNA targets during NES differentiation was confirmed using qPCR with divergent primers with all targets increased ~4 fold or greater as early as day eight of differentiation (D8) **[Fig S6a]**. To determine if these RBPs affected target circRNA expression, we knocked down SFPQ and TIAL1 during NES differentiation with cells treated with siRNA on days zero (NES) and eight (D8) and RNA collected on D8 and D16. For quantification of protein levels, cell lysates were also collected four days after each siRNA treatment **[Fig S6b]**. TIAL1 expression was too low to be detected in any samples, however, SFPQ protein was found to be reduced ~50% at day four compared to non-targeting control siRNA (siNTC) **[Fig S6c,d]**. Similarly, from mRNA quantification, *SFPQ* mRNA was robustly reduced by siRNA treatment while *TIAL1* mRNA levels remained unchanged **[Fig 4e]**. As TIAL1 mRNA levels appeared to be too low during differentiation and unaffected by siRNA treatment, TIAL1, and its targets were excluded from further analyses.

Following siRNA-SFPQ treatment, we quantified the relative expression of select circRNA targets alongside their corresponding linear mRNA form. Knockdown of SFPQ resulted in depletion of all circRNA targets at both D8 and D16 with an apparent greater decrease of circRNAs compared to linear counterparts. This effect was especially pronounced at D16 of differentiation **[Fig 4f]**. Next, two circRNAs that exhibited the greatest decrease following SFPQ knockdown, *circERC2* and *circMYT1L* were selected for *in situ* hybridisation analysis. circRNA probes were designed to hybridise to the back-spliced junction along with a control probe designed to a linear splice junction of one back-spliced exon. No specific signal was seen with a negative scrambledCirc *in situ* probe or for *circMYT1L*, likely due to low expression as linear MYT1L was only detected at low levels **[Fig S7a,b]**. However, *circERC2* was detected with a clear increase in expression observed following differentiation **[Fig 4g-j]**. *In situ* detection of *circERC2* showed outspread co-localised with linear ERC2 and expression throughout the neuronal soma **[Fig 4g-j]**. This localisation pattern also appeared unchanged by siRNA-SFPQ treatment **[Fig S7c-f].** Finally, to determine if SFPQ can bind to the predicted circRNA targets, RNA immunoprecipitation followed by qPCR analysis (RIP-qPCR) was performed on neurons at D28 of differentiation. We found that SFPQ immunoprecipitation enriched all circRNA targets greater than four-fold and, in the case of *circRIMS1_d*, specific enrichment of the circRNA exceeded that of the linear isoform **[Fig 4k]**. Collectively, this suggests a

326 role for SFPQ not only in the regulation of circRNAs during neuronal differentiation but also as a
327 potential binding partner of increased circRNAs.

328

329 *CircRNAs increased during differentiation are flanked by long introns*

330 While the SFPQ targets examined were selected based on enrichment for a singular SFPQ motif,
331 additional motifs for SFPQ are known and could be involved in the effects of SFPQ knockdown.
332 Additionally, SFPQ has previously been shown to have an important role in circRNA biogenesis
333 through interactions with circRNA flanking introns, specifically regulating circRNAs with long flanking
334 introns that contain distal inverted Alu repeat elements (IAE) (Stagsted *et al*, 2021). The observed
335 decrease of circRNA targets following SFPQ knockdown could be due to a more general effect of
336 SFPQ promoting circRNA formation through flanking intronic regions. We, therefore, tested flanking
337 introns of increased circRNAs for enrichment of RBP motifs. Although four motifs for SFPQ were
338 found to be enriched in flanking introns, this represented a small minority among a total of 349
339 enriched motifs from 76 RBPs, the majority of which were motifs corresponding to members of the
340 HNRNP (93) and SRSF (91) protein families **[Table S7d]**. Previously, SFPQ binding sites have been
341 identified as enriched both in close proximity (+/- 2000 bp) to BSJ sites of circRNAs (Stagsted *et al.*,
342 2021) as well at 5' ends of long introns from SFPQ-bound genes (Takeuchi *et al*, 2018). The frequency
343 of SFPQ motifs in flanking introns of circRNA subsets was consequently examined to determine if any
344 position-based pattern was evident. We observed that the frequency of SFPQ motifs among flanking
345 introns of DEcircs is highest at intron ends distal to the BSJ and lowest in regions closest to the BSJ
346 **[Fig 5a]**. Analysing motif position relative to the 5' site of both upstream and downstream flanking
347 introns indicated that this pattern was driven by an enrichment of SFPQ binding sites at 5' intronic
348 sites **[Fig 5b]**. While this indicates that 5' SFPQ motif may be important for biogenesis of circRNAs
349 differentially expressed in this dataset, this pattern was not unique to increased circRNAs and, in fact,
350 circRNAs decreased during differentiation appear to have the highest frequency of 5' SFPQ motifs in
351 their downstream flanking introns.

352 We further compared both flanking intron length and the location of inverted Alu repeats in all
353 circRNAs and circRNAs increased at D28 as potential features of SFPQ-regulated circRNAs. Based
354 on grouping of introns by length and presence of proximal IAEs, the proportion of intronic types was
355 unchanged in the subset of increased circRNAs **[Fig 5c]**. A comparison of mean length, however,
356 found that flanking introns were significantly longer in increased circRNAs ($p = 2.6e-11$) whereas
357 distance to Alu elements in circRNAs that contained IAEs did not differ significantly ($p = 0.1615$) **[Fig**
358 **5d-g]**. These results suggest that intronic length, but not IAE distance, may be an important factor in
359 the increased abundance of circRNAs during NES differentiation.

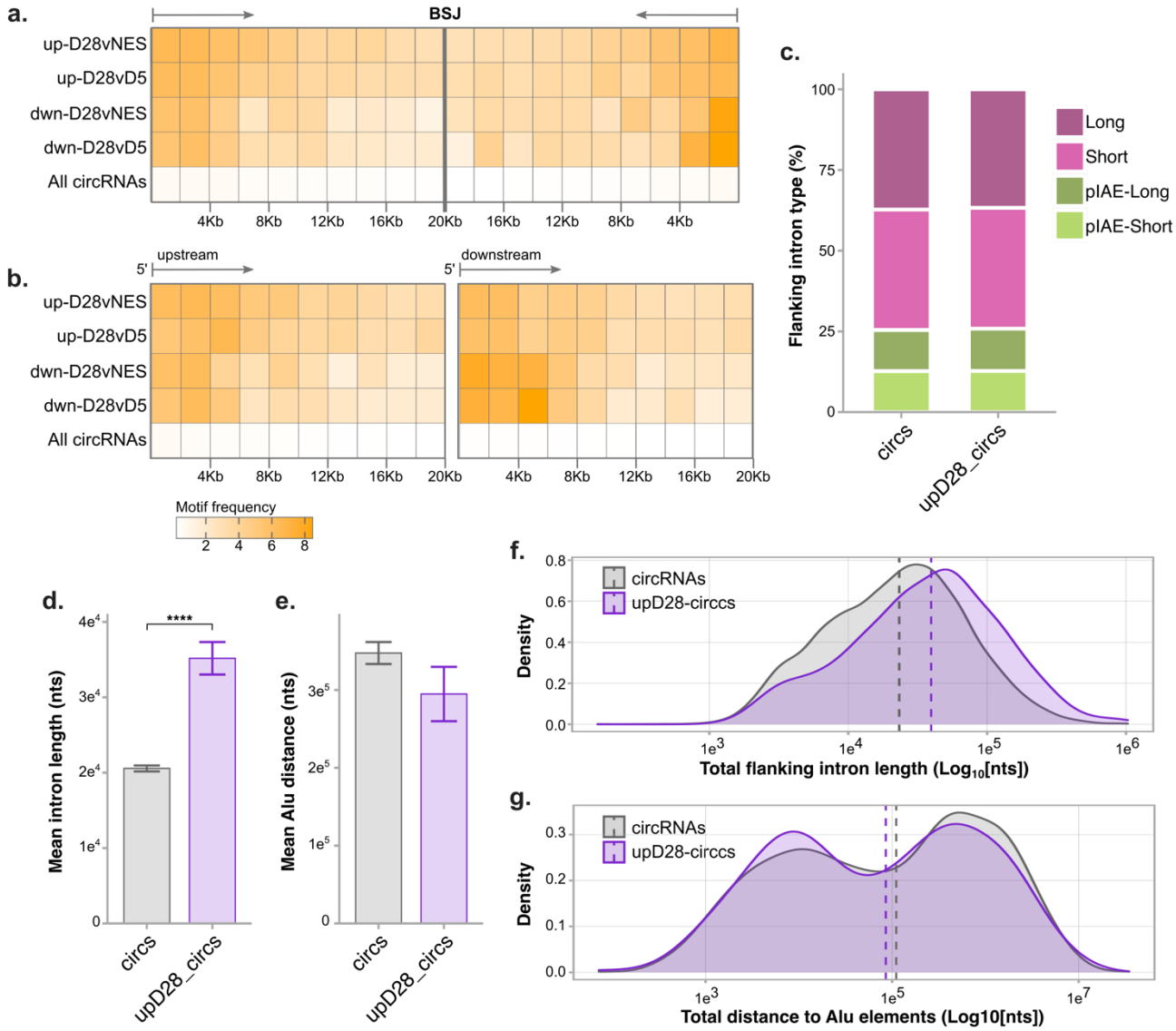

Figure 5. Long introns flank circRNAs increased by NES differentiation. **a.** Frequency of SFPQ motifs in circRNA flanking introns by position relative to intron splice site distal from the BSJ. **b.** Frequency of SFPQ motifs in circRNA flanking introns by position relative to the 5' intron end. Scale in b applies to a and b. **c.** Proportion of flanking intron types among all circRNAs compared to increased circRNAs. Intron types were defined as either, short/long introns with a proximal IAE (pIAE-short/pIAE-long) or short/long introns without proximal IAE (Short/Long). **d.** Mean intron length of flanking introns. **e.** Mean distance to IAE from BSJ. **f.** Density plot of intron length totalled from both flanking introns. **g.** Density plot of IAE distance totalled from Alu element distance on both flanking introns. Error bars in d and e represent standard error, dashed lines in g and f indicate median values. Two sample Z-test, **** = $p < 0.0001$.

374 **Discussion**

375 Despite mounting evidence highlighting an important role for circRNA regulation in normal brain
376 function, our understanding of circRNA generation and function during neurodevelopment remains
377 poorly understood. Our study provides a comprehensive profile of circRNA expression in a human
378 model of neuronal differentiation. Although previous reports have suggested high conservation of
379 circRNAs, more recent evidence indicates that circRNA exons exhibit similar conservation to
380 neighbouring linear exons and that the majority of circRNAs are species-specific with only ~20% of
381 mouse circRNAs having human homologs (Gruhl *et al*, 2021; Guo *et al.*, 2014; Santos-Rodriguez *et*
382 *al*, 2021). Exploring circRNA expression and function within a human-genetic context is therefore
383 critical to understanding the role of circRNAs in both disease and normal brain development.

384 Recent expansions of the human circRNAome also coincide with the creation of various
385 bioinformatic tools for the detection of circRNAs from sequencing of either total RNA or RNA enriched
386 for circRNA by RNase treatment (Hansen, 2018; Sharma *et al*, 2019). Sequencing of circRNA
387 enriched samples offers improvements in detecting lowly expressed circRNAs and the advantage of
388 reconstructing complete circRNA sequences (Rybak-Wolf *et al.*, 2015). By contrast, lowly expressed
389 circRNAs are unlikely to be captured in total RNAseq data, and detection of circRNAs, which relies
390 only on BSJ reads, is prone to false positives. However, the pipeline employed in our study,
391 demonstrates that the identity and expression levels of endogenous circRNAs can be reliably
392 determined from total RNAseq by intersecting results of multiple tools, at least for abundant circRNA
393 species that are most likely to be biologically relevant.

394 An overall pattern of increased circRNA expression following neuronal differentiation has
395 previously been observed in studies of rodent neuronal development, with elevation of circRNAs
396 occurring following neuronal maturation *in vitro* and within the developing mouse hippocampus
397 (Rybak-Wolf *et al.*, 2015; You *et al.*, 2015). Enrichment of GO terms related to neuronal and synaptic
398 functions among hosts of increased circRNAs in our dataset is also consistent with several reports
399 highlighting neuronal genes, and especially synaptic factors, as hosts for numerous circRNAs
400 (Ashwal-Fluss *et al*, 2014; You *et al.*, 2015). Identification of negatively enriched GO terms related to
401 early, but not late differentiation (cell projection/axonogenesis) at D28 vs D5, however, indicates that
402 circRNAs with altered expression arise from host RNAs functioning in biological pathways relevant to
403 the stage of neuronal maturation. We also observed greater relative increases in the levels of
404 circRNAs than in the levels of linear counterparts, supporting prior evidence of specific circRNA
405 regulation during neuronal development. Non-specific accumulation of circRNAs, however, has been
406 reported in non-proliferating cells and with aging in *C. elegans* (Bachmayr-Heyda *et al*, 2015; Cortes-
407 Lopez *et al*, 2018) while brain-specific circRNAs accumulate during aging in more complex organisms

408 like *Drosophila* and mouse (Gruner *et al*, 2016; Westholm *et al*, 2014). Dissecting the mechanisms of
409 both specific circRNA regulation as well as circRNA accumulation will therefore be crucial for
410 understanding circRNA functions in the developing and aging brain.

411 Although mechanisms of circRNA biogenesis are still poorly understood, BSJ formation has
412 been shown to occur co-transcriptionally and appears closely linked to linear mRNA splicing (Ashwal-
413 Fluss *et al.*, 2014). Differential exon usage has been reported to be in competition with exon
414 circularisation (Ashwal-Fluss *et al.*, 2014), whereas other studies identified circRNAs formed primarily
415 from exons with high inclusion rates (Gokool *et al.*, 2020). While we observed a significant increase
416 of alternative splicing among transcripts that host circRNAs, alternative splicing was comparable
417 among host RNAs of increased circRNAs, and no correlation was found between circRNA fold-
418 changes and fold-changes of circularised exons. Pathways enriched among differentially spliced
419 RNAs also diverged from those pathways enriched among host precursors giving rise to circRNAs,
420 the latter featuring processes associated with the ribosome and the spliceosome.

421 Since the majority of individual circRNAs remain unstudied, examining variants occurring in
422 circRNA exons could provide insight into their function and possible roles in evolutionary brain
423 development and disorders. Based on gnomAD data, circRNA exons had slightly higher variant
424 frequency while splice site variant frequency in BSJ exons was significantly lower than nonBSJ exons.
425 We also found that SFARI genes have an increased frequency of rare *de novo* ASD variants in
426 circularised exons. A separate study found a significant enrichment of ASD GWAS SNPs among all
427 circBase circRNAs as well as enrichment of GWAS SNPs for four other traits out of ten tested in total
428 (Rajcsanyi *et al*, 2022). Additionally, numerous SNPs which effect circRNA abundance (circQTLs)
429 have been identified in humans with the majority found to be independent, linked only to circRNA not
430 mRNA expression (Ahmed *et al*, 2019). Further, over 600 independent circQTLs have recently been
431 associated with 389 circRNAs specifically in the ASD brain (Mai *et al*, 2022). Taken together, this
432 indicates that circRNA-forming exons in human may be subject to increased genetic variation, while
433 splice sites of BSJ exons are more constrained. Circularised exons may also be enriched for both
434 common and rare ASD-associated variants and alterations of circRNA function and/or circRNA
435 expression linked to circQTLs may be an important consideration when determining variant effects in
436 ASD.

437 While there is mixed evidence of RBP binding site enrichment in circRNAs (Guo *et al.*, 2014;
438 You *et al.*, 2015), we identified significant enrichment of limited motifs among subsets of DEcircs.
439 SFPQ, found enriched among increased circRNAs, is associated with various aspects of gene
440 regulation and mRNA processing (Heyd & Lynch, 2010; Kaneko *et al*, 2007; Peng *et al*, 2002;
441 Rosonina *et al*, 2005). Though typically localised to nuclear paraspeckles (Passon *et al*, 2012) non-

442 nuclear SFPQ pools, linked to distal axonal transport of RNA granules, have been identified in
443 neuronal cells (Fukuda *et al*, 2021; Furukawa *et al*, 2015; Thomas-Jinu *et al*, 2017). Analogously,
444 SFPQ has been associated with multiple neurodegenerative disorders (Ishigaki *et al*, 2020; Younas
445 *et al*, 2020) and loss of SFPQ causes gross defects in mouse brain development (Takeuchi *et al.*,
446 2018). These effects are associated with defective transcription of long genes, many of which are
447 selectively expressed in the brain, enriched for synaptic functions, and associated with
448 neurodevelopmental disorders (Gabel *et al*, 2015; King *et al*, 2013; Takeuchi *et al.*, 2018). A recent
449 analysis in human cell lines also found that SFPQ knockdown primarily depleted circRNAs with long
450 flanking introns containing distal Alu elements, instead of short introns with proximal Alu elements
451 (Stagsted *et al.*, 2021). Although complementary sequences such as Alu repeats can facilitate
452 circRNA production (Jeck *et al.*, 2013; Westholm *et al.*, 2014), long flanking introns rather than flanking
453 proximal inverted repeats have been shown to be more important in biogenesis of the most abundant
454 and conserved human circRNAs (Stagsted *et al*, 2019; Westholm *et al.*, 2014).

455 We observed that SFPQ appears to be an important player in regulation of circRNAs and,
456 consistent with previously examined SFPQ targets (Stagsted *et al.*, 2021), introns flanking circRNAs
457 increased by NES differentiation were significantly longer than introns flanking all detected circRNAs,
458 while Alu element distance did not appear to be a defining characteristic. Depletion of circRNAs
459 following SFPQ knockdown during differentiation indicates that SFPQ is involved circRNA biogenesis
460 in our model, possibly through previously described mechanisms such as 5' end enriched SFPQ
461 binding in long flanking introns. However, motif enrichment in increased circRNA flanking introns
462 indicates many other RBPs were enriched to a greater extent, and patterns of intronic SFPQ motif
463 enrichment appeared relatively uniform across all DEcircs. This finding indicates that, while SFPQ is
464 likely a critical factor in circRNA biogenesis, additional factors other than intronic SFPQ binding must
465 be involved in directing specific circRNA regulation. Given that SFPQ was uniquely enriched within
466 increased circRNA sequences, we speculate that these exonic binding sites may also play a role in
467 circRNA regulation. Previously, in addition to intronic sites, exonic sites were shown to contribute to
468 circRNA biogenesis from *musclebind like splicing regulator 1* (*MBLN1*) pre-mRNA through binding of
469 its own protein product, MBLN1, thereby regulating its own expression (Ashwal-Fluss *et al.*, 2014).
470 Here, we show that multiple circRNA targets were also enriched by SFPQ immunoprecipitation,
471 suggesting SFPQ binding sites in these circRNAs are occupied and could function in sequestering
472 SFPQ. Further research is needed to untangle the functional significance of SFPQ binding in
473 circRNAs elevated during differentiation either in regulating their own biogenesis, altering host gene
474 splicing and/or sequestering of SFPQ protein.

475 As increasing evidence points to a significant role for circRNAs in neurodevelopment, our data
476 provides an important resource for future studies. We evaluate alternative splicing and differential
477 abundance of linear RNAs and circRNAs and scrutinise genetic variation as well as RBP binding sites,
478 providing an in-depth characterisation of circRNAs in human neuronal differentiation. We also
479 discerned further correlates between circRNAs and neurodevelopmental disorders and identified the
480 splicing factor SFPQ as an important player in neuronal maturation, as both a regulator of circRNA
481 levels and possibly a target itself of circRNA regulation. We note, however, that these mechanisms
482 are not mutually exclusive and a more complex regulatory picture, encompassing splicing modulation,
483 circRNA biogenesis and SFPQ:circRNA binding, is likely yet to be resolved.

484

485 **Materials and methods**

486 *NES cell culture and differentiation*

487 Established neuroepithelial stem (NES) cells, previously derived from a male neurotypical donor
488 (Uhlin *et al*, 2017), were seeded on tissue culture flasks coated with 20 µg/ml poly-L-ornithine (Sigma-
489 Aldrich P3655), and 1 µg/ml laminin (Sigma-Aldrich L2020). Cells were grown in
490 DMEM/F12+GlutaMAX medium (ThermoFisher 31331093) supplemented with 0.05X B27
491 (ThermoFisher 17504044), 1X N2 (ThermoFisher 17502001), 10 ng/ml bFGF (fisher scientific
492 CTP0261), 10 ng/ml EGF (PeproTech AF-100-15) and 10 U/ml penicillin/streptomycin (ThermoFisher
493 15140122). Medium was exchanged 50% daily and cells maintained in 5% CO_2 at 37°C, passaging
494 once 100% confluent and seeding at a density of $5x10^4$ cells/cm^2. Neural differentiation was induced
495 by growth factor withdrawal the day after plating with media B27 concentration increased to 0.5X.
496 Media was exchanged 50% every second day up until D15, after which media was supplemented with
497 0.4 ug/ml laminin and exchanged 50% every three days.

498

499 *RNA extraction and RNA sequencing*

500 Cells were lysed in TRIzol reagent (ThermoFischer 15596026) before separating with chloroform and
501 mixing the aqueous phase with isopropanol as per manufacturer directions. RNA was then isolated
502 from the isopropanol/chloroform solution using the ReliaPrep RNA Cell Miniprep kit (Promega Z6010).
503 Three to five biological replicates were extracted for each cell line and time point. Libraries were
504 prepared with Illumina Truseq Stranded total RNA RiboZero GOLD kit and sequenced on the
505 NovaSeq6000 platform with a 2x151 setup using NovaSeqXp workflow in S4 mode flowcell. Raw
506 reads were processed using cutadapt v3.2 to trim adaptor sequences and low-quality base pairs and

507 discard short reads (options: -m 20 -e 0.1 -q 20 -O 1). The GRCh37 genome assembly was used for
508 all alignment, annotation, and downstream analysis steps.

509

510 *CircRNA detection from RNAseq*

511 Back-spliced junctions were detected from paired end reads using three separate programs;
512 CIRCexplorer2 v2.3.8 (Zhang *et al*, 2016), MapSplice2 v2.1.8 (Wang *et al*, 2010) and CIRI2 v2.0.6
513 (Gao *et al*, 2018). For CIRCexplorer2, modules were run with default options, reads were pre-aligned
514 with TopHat v2.0.9 tophat_fusion (with Bowtie v1.1.2 and Samtools v0.1.19) using –fusion-min-dist
515 200. MapSplice was run using python v2.7.6 and options –fusion-non-canonical –min-fusion-dist 200.
516 CIRI2 was run using Perl v5.26.2 with default settings after aligning reads with BWA v0.7.17 (with
517 Samtools v1.9). The R package circRNAprofiler v1.4.2 (Aufiero *et al*, 2020) was used as described in
518 the manual to merge and filter back-spliced junction reads from all three detection programs as well
519 as for circRNA annotation and extraction of circRNA sequences.

520

521 *Differential expression and gene ontology analyses*

522 Based on clustering analysis, two outlier samples (1xNES/1xD5) were initially removed before
523 differential expression analysis of both circRNAs and genes using DESeq2 v1.30.1 and applying the
524 ashr method of log fold-change shrinkage (lfc-shrink) (Stephens, 2017). Thresholds of lfc-shrink
525 values ≥ |2| and p-adjusted <0.05 were used for sub-setting circRNAs and genes as differentially
526 expressed. For analysis of expression over all three time points, results from DESeq2 likelihood ratio
527 test were analysed with DEGreport v1.26.0. Analysis of differential exon usage was performed using
528 the DEXSeq package (v1.40.0) (Anders *et al*, 2012) using provided python scripts to generate a
529 flattened annotation file of exon bins, with aggregation disabled, and to count reads within exon bins.
530 The standard analysis pipeline described in the tutorial was followed, defining exon bins as
531 differentially used if estimated log fold-change was ≥|2|, padj <0.05 and exon base mean >10 and
532 classifying genes as differentially spliced if at least one exon of a gene was differentially used. As
533 some exon bins defined by DEXSeq differed from annotated exon regions, differential exon usage
534 data was compared with circRNA exons based on position information and using the intersect function
535 of bedtools software v2.29.2. For annotated exons which contained multiple exon bins, exon fold-
536 changes were calculated as the mean estimated exon bin fold-change. The clusterProfiler package
537 v3.18.1 was used for all gene ontology analyses using either biological process terms annotated in
538 org.Hs.eg.db v3.12.0 or user input annotations for analysis of NDD-associated gene enrichment. As
539 GSEA requires only one entry per gene and numerous host genes had multiple circRNAs, data were

540 split into negatively and positively regulated circRNAs and the minimum and maximum circRNA lfc-
541 shrink values were assigned to host genes with duplicate entries.

542

543 *PCR, quantitative PCR and Sanger sequencing validation of circRNAs*

544 For all experiments, cDNA was generated using the iScript cDNA synthesis kit (Bio-Rad). To validate
545 circRNA detection, divergent primers **[Fig S1b]** were designed as previously described (Panda &
546 Gorospe, 2018). PCR was performed using HotStarTaq (Qiagen) and bands visualized by gel
547 electrophoresis. For Sanger sequencing, sequences were amplified using HotStarTaq and circular
548 primers **[Fig S1b]**. Products were isolated using DNA Clean and Concentrator-5 kit (Zymo Research)
549 or, if multiple products, bands were separated using gel electrophoresis and extracted using
550 Zymoclean Gel DNA Recovery Kit (Zymo Research). Samples were sequenced by Eurofins Scientific
551 before comparing alignments to predicted annotations with nucleotide BLAST and visualizing
552 alignments with ApE v2.0.49.0. Divergent primers and SYBR green (Bio-Rad) were used for
553 quantitative PCR (qPCR) analyses. For differential expression validation, ciRNA expression was
554 normalised to two reference circRNAs, *circRTN4* and *circCASK1G3,* found to have high and
555 consistent expression throughout NES differentiation. For siRNA experiments, all circRNAs were
556 normalized to *U6* snRNA and all genes/linear RNAs were normalised to *GAPDH* mRNA. For known
557 circRNAs, divergent BSJ primers were designed using circInteractome (Dudekula *et al*, 2016). For
558 novel circRNA divergent BSJ junctions and for all circRNA primers, circRNA sequences were
559 recreated in SnapGene Viewer v5.1.1 based on annotations from circRNAprofiler and exon
560 sequences in Ensembl GRCh37 and primers designed using NCBI primer blast. All primer sequences
561 are listed in **Table S8**.

562

563 *Variant Analysis*

564 For circRNAs which annotated to known splice sites, exon regions were extracted based on the
565 longest transcript containing the upstream and downstream back-spliced exons and sub-grouped as
566 in **Fig 3a**, with the assumption that no exons were spliced out of circRNAs. GnomAD GRCh37 exomes
567 files v2.1.1 were downloaded for each chromosome and converted into bed format. *De novo* variants
568 associated with ASD cases and controls were sourced from Satterstrom *et al.* (2020) and SCZ
569 variants were pooled from various sources listed in **Table S5**. All variants were intersected with exon
570 subgroups using bedtools and all downstream analysis was performed in R, normalising all exon
571 variant frequencies by exon length. SIFT annotations for gnomAD exon variants were predicted using
572 Ensembl VEP v104.

573 *miRNA and RBP binding site prediction*

574 A list of 125 miRNAs associated with neurodevelopment or NDDs **[Table S6a,b]** was collated from
575 literature review and pubmed searches for miRNA/microRNA with terms such as
576 neurodevelopment/neuronal/neuron differentiation etc. Ensembl biomart was used to extract 3'UTR
577 sequences for DEGs and, if multiple 3'UTR sequences were annotated to a single gene, the longest
578 3'UTR sequence was used. miRNA binding sites in circRNA and 3'UTR sequences were predicted
579 using remote RNA22 v2 with the following parameters: seedmismatchesallowed = 0; seedsize = 8;
580 minpairmatchs = 12; minenergy = -12; maxguwobbles = 1; threshold = 7000000. To examine
581 enrichment of RNA-binding motifs in circRNAs, separate fasta files of DEcircs were generated for
582 circRNAs decreased or increased at D28vNES / D28vD5 and D5vNES as well as all 4 LRT clusters.
583 RNA-binding protein motifs were downloaded from the ATtRACT database v0.99β. Motif enrichment
584 was tested using the AME function of MEME-suite v5.3.0 with default settings and a background
585 dataset of all annotated (5839/6385) circRNAs. For individual motif site detection, the MEME-suite
586 FIMO function was used with a threshold p-value of 0.001.

587

588 *siRNA mediated silencing and protein detection*

589 For siRNA mediated knockdown, Accell Human SMARTpool siRNAs targeting SFPQ (E-006455-00-
590 0010) or TIAL1 (E-011405-00-0010) were added to cell media at a final concentration of 0.3 µM.
591 Accell non-targeting control pool (D-001910-10-20), transfected at the same concentration was used
592 as a control treatment (siNTC). Protein samples were collected 96 hr after siRNA treatment. After
593 removing media and washing once with PBS cells collected with a cell scraper in a lysis buffer of 50
594 nM Tris-HCl, 100 mM 100 mM NaCl, 5 mM EDTA, 1 mM EGTA and 1X HALT protease inhibitor
595 cocktail (PIC; Fischer Scientific) and samples sonicated at 36% amplitude for 6X 1 sec. The Qubit
596 Protein Assay Kit (Thermo Scientific) was used to measure protein concentration. Protein was
597 detected using the Simple-Western-JESS capillary western blot system (Bio Techne) multiplexed for
598 total protein and chemiluminescence detection of mouse αSFPQ (1:2000; Sigma-Aldrich
599 WH0006421M2) or mouse αTIAL1 (1:10; Santa Cruz sc-398372). The Compass for S.W. software
600 v5.0.1 was used to analyse data and calculate peak area normalised to total protein area.

601

602 *In Situ Hybridisation*

603 Locked nucleic acid (LNA) probes for *in situ* were designed to be 45-55 bps in length with a melting
604 temperature of ~70-75°C. Probes were designed to be complementary to the BSJ for circRNA

605 detection while linear control probes were designed to target a linear splice junction, within the same
606 transcript, containing one of the BSJ exons. CircRNA probes plus a negative control scrambled
607 circRNA probe labelled with 5'FAM and linear probes labelled with 5'Cy3 were ordered from
608 Integrated DNA Technologies (IDT) as HPLC purified, Affinity Plus DNA oligos and resuspended in
609 TE buffer. Details of all probe sequences are listed in **Table S9**. Cells were plated on glass coverslips
610 coated with 100 µg/ml poly-L-ornithine and 2 µg/ml laminin. *In situ* hybridisation was performed as
611 described previously with some modifications (Zirkel & Papantonis, 2018). Cells were washed with
612 PBS before incubation in fresh fixative (4% PFA, 0.9% NaCl and 5% Glacial acetic acid in UltraPure
613 H_2O) for 17 min at room temp. Coverslips were washed for 5 min with PBS before adding ice-cold
614 70% ethanol and storing at least overnight or up to a few weeks at -20°C. After removing from -20°C
615 cells were recovered for 5 min at room temp in PBS, permeabilised for 10 min in 0.5% Triton X-
616 100/0.5% saponin (Sigma-Aldrich S7900) and washed in PBS. Cells were then treated with 1%
617 formaldehyde in PBS for 10 min and washed once in PBS for 10 min. Cells were dehydrated with
618 ethanol at 70, 90 and 100% for 3 min each and air-dried. For each coverslip 15 ng of labelled probe
619 was diluted in 50 µL of hybridisation buffer consisting of 10% Dextran sulfate (Sigma-Aldrich 265152),
620 0.1% Sodium dodecyl sulfate (Sigma-Aldrich 71736), 30% Ethylene carbonate (Sigma-Aldrich
621 E26258), 20 µg/mL Yeast tRNA (Thermo Fischer AM7119) and 2X SSC. Probes were denatured at
622 83°C for 5 min and hybridised overnight at 37°C in a box humidified with 2X SSC. Coverslips were
623 washed 3 times in 2X SSC for 10 min at 42°C, followed by two 3-min PBS washes at room temp.
624 Cells were blocked for 30 min in 0.1% Triton X/5% Donkey serum/PBS and counterstained with
625 1:1000 Hoechst. After two 3-min washes in PBS, coverslips were air-dried for 3-5 min and mounted
626 onto glass slides using Prolong Diamond Antifade Mountant (Thermo Fischer). Images were acquired
627 using an LSM 700 Zeiss Confocal Microscope and contrast was enhanced uniformly.

628

629 *Formaldehyde RNA immunoprecipitation*

630 Formaldehyde RNA immunoprecipitation (fRIP) was performed as previously described (Hendrickson
631 *et al*, 2016) with some modifications. NES cells were differentiated until D28 in a T75 flask. To collect,
632 cells were washed with PBS, rinsed with 6 mL Accutase for 10 sec and incubated in 4 mL TrypLE
633 select for 2 min/37°C before addition of 200 µL of Neuronal isolation enzyme (Thermo Scientific,
634 88285) and further incubating 1 min/37°C. Dissociation was stopped with 6 mL of Trypsin inhibitor
635 and solution collected, any remaining cells were collected by rinsing flasks with 6 mL of Wash Medium
636 (DMEM/F12+GlutaMAX, 5% FBS, 10 U/ml penicillin/streptomycin). Clumps were broken up by gentle
637 pipetting and cells spun at 400 x g for 3 min and resuspended in Wash Medium at $5x10^6$ cells/mL.
638 Crosslinking was performed by addition of formaldehyde to a final concentration of 0.1% and

639 incubation for 10 min with rotation. Glycine was added at a concentration of 125 mM, incubating for 5
640 min with rotation to stop the reaction. Cells were pelleted, washed twice in cold PBS and once in PIC,
641 and stored at -80°C. For immunoprecipitation, cell pellets were resuspended and lysed by incubation
642 for 10 min at 4 °C with rotation in RIPA lysis buffer (50 mM TRIS [pH 8], 150 mM KCL, 0.1% SDS, 1%
643 Triton-X, 5 mM EDTA, 0.5% sodium deoxycholate, 0.5 mM DTT, 1X PIC, 100 U/mL RNaseOUT). The
644 lysate was sonicated 15 times (0.7s on, 1.3s off, Vibra-Cell VCX-600, Sonics) at an amplitude of 10%
645 and centrifuged at max speed for 10 min at 4°C. Supernatant was collected and diluted with an equal
646 volume of Binding buffer (150 mM KCl, 25 mM Tris [pH 7.5], 5 mM EDTA, 0.5 % IGEPAL) with 0.5
647 mM DTT, 1X PIC and 100 U/mL RNaseOUT added. Cells were incubated 2 hr at 4°C with rotation
648 after addition of either 6 µg mouse αSFPQ (Sigma-Aldrich WH0006421M2) or 6 µg normal mouse
649 αIgG (Santa Cruz sc-2025). To each immunoprecipitation, 50 µL of Dynabeads Protein G (Thermo
650 Fischer 10004D), pre-washed 2X in Binding buffer, was added before incubating 1 hr/4°C with
651 rotation. Beads were washed 2X 10 min/4°C with rotation in 1 mL Binding buffer/PIC/RNaseOUT. To
652 reverse cross-linking, beads were resuspended in 56 µL UltraPure water and 33 µL reverse
653 crosslinking buffer (PBS (without Mg or Ca), 6% N-lauroyl sarcosine, 30 mM EDTA, 15 mM DTT), 2
654 mg/mL Proteinase K and 400 U/mL RNaseOUT were added to each reaction, before incubating 1
655 hr/42°C followed by 1 hr/55°C. Bead/buffer mix was added to 1 mL TRIzol and RNA extraction
656 performed as described above. For each fRIP, 5 ng of RNA was used for cDNA synthesis and targets
657 were analysed by qPCR, normalizing SFPQ-fRIP to IgG-fRIP.

658

659 *Intron Analysis*

660 Sequences for introns flanking circRNA back-spliced exons were extracted using BSgenome v1.58.0
661 and Biostrings v2.58.0 based on annotations output by circRNAprofiler. RBP binding sites were
662 predicted using MEME-suite as described above and SFPQ motif frequency for each subset of
663 circRNAs normalised by the number of circRNAs. All GRCh37 repeat elements were downloaded
664 from UCSC table browser RepeatMasker track and Alu elements extracted using grep. Bedtools
665 intersect was used to subset Alu elements that overlapped with intronic regions by at least 50% of the
666 repeat element length and bedtools closest tool used to find Alu elements closest to the BSJ site.
667 CircRNAs were classified as having inverted Alu elements when the closest Alu elements in the
668 downstream and upstream flanking introns were in opposite orientation (on opposite strands).
669 CircRNAs were classified as having proximal IAE flanking introns based on a total Alu distance from
670 the BSJ less than the median for all circRNAs with IAEs. Classification of circRNAs with short or long
671 flanking introns was also classified based on median length, totalled from both flanking introns.

672

673 *Statistics and Data Visualisation*

674 All statistics and data visualisation were performed in R v4.0.4. Specific statistical tests performed are
675 described within the relevant results section. Various R packages were used for visualisation of data
676 including ggplot2 v3.3.3, EnhancedVolcano v1.8.0 and VennDiagram v1.6.20

677

678 **Acknowledgments**

679 The authors acknowledge support from the National Genomics Infrastructure in Stockholm funded by
680 Science for Life Laboratory, the Knut and Alice Wallenberg Foundation and the Swedish Research
681 Council, the SNIC/Uppsala Multidisciplinary Center for Advanced Computational Science for
682 assistance with massively parallel sequencing and access to the UPPMAX computational
683 infrastructure, and the iPS Core facility at Karolinska Institutet for assistance with the generation of
684 iPSC and NES cells. The project was supported by the Swedish Research Council (KT), Swedish
685 Foundation for Strategic Research (KT), the Swedish Brain Foundation – Hjärnfonden (KT),, Strategic
686 Research Area Neuroscience Stratneuro (KT, MW), The Swedish Foundation for International
687 Cooperation in Research and Higher Education STINT (KT), The Wenner Gren Foundation (MW),
688 Sällskapet Barnavård (MW), the Board of Research at Karolinska Institutet (KT) and the National
689 Institute of Aging's Intramural Research Program, National Institutes of Health (MG). Open access
690 funding provided by Karolinska Institutet.

691

692 **Competing Interests**

693 The authors have no competing interests to declare.

694

695 **References**

696 Ahmed I, Karedath T, Al-Dasim FM, Malek JA (2019) Identification of human genetic variants
697 controlling circular RNA expression. *RNA* 25: 1765-1778
698 Anders S, Reyes A, Huber W (2012) Detecting differential usage of exons from RNA-seq data.
699 *Genome Res* 22: 2008-2017
700 Ashwal-Fluss R, Meyer M, Pamudurti NR, Ivanov A, Bartok O, Hanan M, Evantal N, Memczak S,
701 Rajewsky N, Kadener S (2014) circRNA biogenesis competes with pre-mRNA splicing. *Mol Cell*
702 56: 55-66

703 Aufiero S, Reckman YJ, Tijsen AJ, Pinto YM, Creemers EE (2020) circRNAprofiler: an R-based
704 computational framework for the downstream analysis of circular RNAs. *BMC Bioinformatics* 21:
705 164
706 Bachmayr-Heyda A, Reiner AT, Auer K, Sukhbaatar N, Aust S, Bachleitner-Hofmann T, Mesteri I,
707 Grunt TW, Zeillinger R, Pils D (2015) Correlation of circular RNA abundance with proliferation--
708 exemplified with colorectal and ovarian cancer, idiopathic lung fibrosis, and normal human tissues.
709 *Sci Rep* 5: 8057
710 Barbagallo D, Caponnetto A, Brex D, Mirabella F, Barbagallo C, Lauretta G, Morrone A, Certo F,
711 Broggi G, Caltabiano R *et al* (2019) CircSMARCA5 Regulates VEGFA mRNA Splicing and
712 Angiogenesis in Glioblastoma Multiforme Through the Binding of SRSF1. *Cancers (Basel)* 11
713 Becker M, Mastropasqua F, Reising JP, Maier S, Ho ML, Rabkina I, Li D, Neufeld J, Ballenberger L,
714 Myers L *et al* (2020) Presynaptic dysfunction in CASK-related neurodevelopmental disorders.
715 *Transl Psychiatry* 10: 312
716 Chen BJ, Huang S, Janitz M (2019) Changes in circular RNA expression patterns during human foetal
717 brain development. *Genomics* 111: 753-758
718 Chen YJ, Chen CY, Mai TL, Chuang CF, Chen YC, Gupta SK, Yen L, Wang YD, Chuang TJ (2020)
719 Genome-wide, integrative analysis of circular RNA dysregulation and the corresponding circular
720 RNA-microRNA-mRNA regulatory axes in autism. *Genome Res* 30: 375-391
721 Cocquerelle C, Daubersies P, Majerus MA, Kerckaert JP, Bailleul B (1992) Splicing with inverted order
722 of exons occurs proximal to large introns. *EMBO J* 11: 1095-1098
723 Conn VM, Hugouvieux V, Nayak A, Conos SA, Capovilla G, Cildir G, Jourdain A, Tergaonkar V,
724 Schmid M, Zubieta C *et al* (2017) A circRNA from SEPALLATA3 regulates splicing of its cognate
725 mRNA through R-loop formation. *Nat Plants* 3: 17053
726 Cortes-Lopez M, Gruner MR, Cooper DA, Gruner HN, Voda AI, van der Linden AM, Miura P (2018)
727 Global accumulation of circRNAs during aging in Caenorhabditis elegans. *BMC Genomics* 19: 8
728 Das A, Rout PK, Gorospe M, Panda AC (2019) Rolling Circle cDNA Synthesis Uncovers Circular RNA
729 Splice Variants. *Int J Mol Sci* 20
730 Dell'Orco M, Elyaderani A, Vannan A, Sekar S, Powell G, Liang WS, Neisewander JL, Perrone-
731 Bizzozero NI (2021) HuD Regulates mRNA-circRNA-miRNA Networks in the Mouse Striatum
732 Linked to Neuronal Development and Drug Addiction. *Biology (Basel)* 10
733 Dolmetsch R, Geschwind DH (2011) The human brain in a dish: the promise of iPSC-derived neurons.
734 *Cell* 145: 831-834
735 Du WW, Yang W, Liu E, Yang Z, Dhaliwal P, Yang BB (2016) Foxo3 circular RNA retards cell cycle
736 progression via forming ternary complexes with p21 and CDK2. *Nucleic Acids Res* 44: 2846-2858

737 Dudekula DB, Panda AC, Grammatikakis I, De S, Abdelmohsen K, Gorospe M (2016)
738 CircInteractome: A web tool for exploring circular RNAs and their interacting proteins and
739 microRNAs. *RNA Biol* 13: 34-42
740 Fukuda Y, Pazyra-Murphy MF, Silagi ES, Tasdemir-Yilmaz OE, Li Y, Rose L, Yeoh ZC, Vangos NE,
741 Geffken EA, Seo HS *et al* (2021) Binding and transport of SFPQ-RNA granules by KIF5A/KLC1
742 motors promotes axon survival. *J Cell Biol* 220
743 Furukawa MT, Sakamoto H, Inoue K (2015) Interaction and colocalization of HERMES/RBPMS with
744 NonO, PSF, and G3BP1 in neuronal cytoplasmic RNP granules in mouse retinal line cells. *Genes*
745 *Cells* 20: 257-266
746 Gabel HW, Kinde B, Stroud H, Gilbert CS, Harmin DA, Kastan NR, Hemberg M, Ebert DH, Greenberg
747 ME (2015) Disruption of DNA-methylation-dependent long gene repression in Rett syndrome.
748 *Nature* 522: 89-93
749 Gao Y, Zhang J, Zhao F (2018) Circular RNA identification based on multiple seed matching. *Brief*
750 *Bioinform* 19: 803-810
751 Glazar P, Papavasileiou P, Rajewsky N (2014) circBase: a database for circular RNAs. *RNA* 20: 1666-
752 1670
753 Gokool A, Anwar F, Voineagu I (2020) The Landscape of Circular RNA Expression in the Human
754 Brain. *Biol Psychiatry* 87: 294-304
755 Gruhl F, Janich P, Kaessmann H, Gatfield D (2021) Circular RNA repertoires are associated with
756 evolutionarily young transposable elements. *Elife* 10
757 Gruner H, Cortes-Lopez M, Cooper DA, Bauer M, Miura P (2016) CircRNA accumulation in the aging
758 mouse brain. *Sci Rep* 6: 38907
759 Guo JU, Agarwal V, Guo H, Bartel DP (2014) Expanded identification and characterization of
760 mammalian circular RNAs. *Genome Biol* 15: 409
761 Hansen TB (2018) Improved circRNA Identification by Combining Prediction Algorithms. *Front Cell*
762 *Dev Biol* 6: 20
763 Hendrickson DG, Kelley DR, Tenen D, Bernstein B, Rinn JL (2016) Widespread RNA binding by
764 chromatin-associated proteins. *Genome Biol* 17: 28
765 Heyd F, Lynch KW (2010) Phosphorylation-dependent regulation of PSF by GSK3 controls CD45
766 alternative splicing. *Mol Cell* 40: 126-137
767 Hollensen AK, Thomsen HS, Lloret-Llinares M, Kamstrup AB, Jensen JM, Luckmann M, Birkmose N,
768 Palmfeldt J, Jensen TH, Hansen TB *et al* (2020) circZNF827 nucleates a transcription inhibitory
769 complex to balance neuronal differentiation. *Elife* 9

770 Ishigaki S, Riku Y, Fujioka Y, Endo K, Iwade N, Kawai K, Ishibashi M, Yokoi S, Katsuno M, Watanabe
771 H *et al* (2020) Aberrant interaction between FUS and SFPQ in neurons in a wide range of FTLD
772 spectrum diseases. *Brain* 143: 2398-2405
773 Jeck WR, Sorrentino JA, Wang K, Slevin MK, Burd CE, Liu J, Marzluff WF, Sharpless NE (2013)
774 Circular RNAs are abundant, conserved, and associated with ALU repeats. *RNA* 19: 141-157
775 Kaneko S, Rozenblatt-Rosen O, Meyerson M, Manley JL (2007) The multifunctional protein
776 p54nrb/PSF recruits the exonuclease XRN2 to facilitate pre-mRNA 3' processing and transcription
777 termination. *Genes Dev* 21: 1779-1789
778 King IF, Yandava CN, Mabb AM, Hsiao JS, Huang HS, Pearson BL, Calabrese JM, Starmer J, Parker
779 JS, Magnuson T *et al* (2013) Topoisomerases facilitate transcription of long genes linked to autism.
780 *Nature* 501: 58-62
781 Li D, Choque Olsson N, Becker M, Arora A, Jiao H, Norgren N, Jonsson U, Bolte S, Tammimies K
782 (2022a) Rare variants in the outcome of social skills group training for autism. *Autism Res* 15: 434-
783 446
784 Li W, Shan B, Cheng X, He H, Qin J, Zhao H, Tian M, Zhang X, Jin G (2022b) circRNA Acbd6
785 promotes neural stem cell differentiation into cholinergic neurons via the miR-320-5p-Osbpl2 axis.
786 *J Biol Chem* 298: 101828
787 Liu Z, Wu X, Yu Z, Tang X (2021) Reconstruction of circRNA-miRNA-mRNA associated ceRNA
788 networks reveal functional circRNAs in intracerebral hemorrhage. *Sci Rep* 11: 11584
789 Ma N, Pan J, Ye X, Yu B, Zhang W, Wan J (2019) Whole-Transcriptome Analysis of APP/PS1 Mouse
790 Brain and Identification of circRNA-miRNA-mRNA Networks to Investigate AD Pathogenesis. *Mol*
791 *Ther Nucleic Acids* 18: 1049-1062
792 Mahmoudi E, Fitzsimmons C, Geaghan MP, Shannon Weickert C, Atkins JR, Wang X, Cairns MJ
793 (2019) Circular RNA biogenesis is decreased in postmortem cortical gray matter in schizophrenia
794 and may alter the bioavailability of associated miRNA. *Neuropsychopharmacology* 44: 1043-1054
795 Mai TL, Chen CY, Chen YC, Chiang TW, Chuang TJ (2022) Trans-genetic effects of circular RNA
796 expression quantitative trait loci and potential causal mechanisms in autism. *Mol Psychiatry*
797 Memczak S, Jens M, Elefsinioti A, Torti F, Krueger J, Rybak A, Maier L, Mackowiak SD, Gregersen
798 LH, Munschauer M *et al* (2013) Circular RNAs are a large class of animal RNAs with regulatory
799 potency. *Nature* 495: 333-338
800 Nigro JM, Cho KR, Fearon ER, Kern SE, Ruppert JM, Oliner JD, Kinzler KW, Vogelstein B (1991)
801 Scrambled exons. *Cell* 64: 607-613
802 Panda AC, Gorospe M (2018) Detection and Analysis of Circular RNAs by RT-PCR. *Bio Protoc* 8
803 Panda AC, Grammatikakis I, Munk R, Gorospe M, Abdelmohsen K (2017) Emerging roles and context
804 of circular RNAs. *Wiley Interdiscip Rev RNA* 8

805 Pandey PR, Yang JH, Tsitsipatis D, Panda AC, Noh JH, Kim KM, Munk R, Nicholson T, Hanniford D,
806 Argibay D *et al* (2020) circSamd4 represses myogenic transcriptional activity of PUR proteins.
807 *Nucleic Acids Res* 48: 3789-3805
808 Passon DM, Lee M, Rackham O, Stanley WA, Sadowska A, Filipovska A, Fox AH, Bond CS (2012)
809 Structure of the heterodimer of human NONO and paraspeckle protein component 1 and analysis
810 of its role in subnuclear body formation. *Proceedings of the National Academy of Sciences of the*
811 *United States of America* 109: 4846-4850
812 Peng R, Dye BT, Perez I, Barnard DC, Thompson AB, Patton JG (2002) PSF and p54nrb bind a
813 conserved stem in U5 snRNA. *RNA* 8: 1334-1347
814 Piwecka M, Glazar P, Hernandez-Miranda LR, Memczak S, Wolf SA, Rybak-Wolf A, Filipchyk A,
815 Klironomos F, Cerda Jara CA, Fenske P *et al* (2017) Loss of a mammalian circular RNA locus
816 causes miRNA deregulation and affects brain function. *Science* 357
817 Rahimi K, Veno MT, Dupont DM, Kjems J (2021) Nanopore sequencing of brain-derived full-length
818 circRNAs reveals circRNA-specific exon usage, intron retention and microexons. *Nature*
819 *communications* 12: 4825
820 Rajcsanyi LS, Diebels I, Pastoors L, Kanber D, Peters T, Volckmar AL, Zheng Y, Grosse M, Dieterich
821 C, Hebebrand J *et al* (2022) Evidence for correlations between BMI-associated SNPs and
822 circRNAs. *Sci Rep* 12: 12643
823 Rosonina E, Ip JY, Calarco JA, Bakowski MA, Emili A, McCracken S, Tucker P, Ingles CJ, Blencowe
824 BJ (2005) Role for PSF in mediating transcriptional activator-dependent stimulation of pre-mRNA
825 processing in vivo. *Mol Cell Biol* 25: 6734-6746
826 Rybak-Wolf A, Stottmeister C, Glazar P, Jens M, Pino N, Giusti S, Hanan M, Behm M, Bartok O,
827 Ashwal-Fluss R *et al* (2015) Circular RNAs in the Mammalian Brain Are Highly Abundant,
828 Conserved, and Dynamically Expressed. *Mol Cell* 58: 870-885
829 Salzman J, Chen RE, Olsen MN, Wang PL, Brown PO (2013) Cell-type specific features of circular
830 RNA expression. *PLoS Genet* 9: e1003777
831 Salzman J, Gawad C, Wang PL, Lacayo N, Brown PO (2012) Circular RNAs are the predominant
832 transcript isoform from hundreds of human genes in diverse cell types. *PLoS One* 7: e30733
833 Santos-Rodriguez G, Voineagu I, Weatheritt RJ (2021) Evolutionary dynamics of circular RNAs in
834 primates. *Elife* 10
835 Satterstrom FK, Kosmicki JA, Wang J, Breen MS, De Rubeis S, An JY, Peng M, Collins R, Grove J,
836 Klei L *et al* (2020) Large-Scale Exome Sequencing Study Implicates Both Developmental and
837 Functional Changes in the Neurobiology of Autism. *Cell* 180: 568-584 e523
838 Sharma D, Sehgal P, Hariprakash J, Sivasubbu S, Scaria V (2019) Methods for Annotation and
839 Validation of Circular RNAs from RNAseq Data. *Methods Mol Biol* 1912: 55-76

840 Stagsted LV, Nielsen KM, Daugaard I, Hansen TB (2019) Noncoding AUG circRNAs constitute an
841 abundant and conserved subclass of circles. *Life Sci Alliance* 2
842 Stagsted LVW, O'Leary ET, Ebbesen KK, Hansen TB (2021) The RNA-binding protein SFPQ
843 preserves long-intron splicing and regulates circRNA biogenesis in mammals. *Elife* 10
844 Stephens M (2017) False discovery rates: a new deal. *Biostatistics* 18: 275-294
845 Suenkel C, Cavalli D, Massalini S, Calegari F, Rajewsky N (2020) A Highly Conserved Circular RNA
846 Is Required to Keep Neural Cells in a Progenitor State in the Mammalian Brain. *Cell Rep* 30: 2170-
847 2179 e2175
848 Takeuchi A, Iida K, Tsubota T, Hosokawa M, Denawa M, Brown JB, Ninomiya K, Ito M, Kimura H,
849 Abe T *et al* (2018) Loss of Sfpq Causes Long-Gene Transcriptopathy in the Brain. *Cell Rep* 23:
850 1326-1341
851 Thomas-Jinu S, Gordon PM, Fielding T, Taylor R, Smith BN, Snowden V, Blanc E, Vance C, Topp S,
852 Wong CH *et al* (2017) Non-nuclear Pool of Splicing Factor SFPQ Regulates Axonal Transcripts
853 Required for Normal Motor Development. *Neuron* 94: 931
854 Tsitsipatis D, Grammatikakis I, Driscoll RK, Yang X, Abdelmohsen K, Harris SC, Yang JH, Herman
855 AB, Chang MW, Munk R *et al* (2021) AUF1 ligand circPCNX reduces cell proliferation by competing
856 with p21 mRNA to increase p21 production. *Nucleic Acids Res* 49: 1631-1646
857 Uhlin E, Ronnholm H, Day K, Kele M, Tammimies K, Bolte S, Falk A (2017) Derivation of human iPS
858 cell lines from monozygotic twins in defined and xeno free conditions. *Stem Cell Res* 18: 22-25
859 Veno MT, Hansen TB, Veno ST, Clausen BH, Grebing M, Finsen B, Holm IE, Kjems J (2015) Spatio-
860 temporal regulation of circular RNA expression during porcine embryonic brain development.
861 *Genome Biol* 16: 245
862 Wang K, Singh D, Zeng Z, Coleman SJ, Huang Y, Savich GL, He X, Mieczkowski P, Grimm SA, Perou
863 CM *et al* (2010) MapSplice: accurate mapping of RNA-seq reads for splice junction discovery.
864 *Nucleic Acids Res* 38: e178
865 Westholm JO, Miura P, Olson S, Shenker S, Joseph B, Sanfilippo P, Celniker SE, Graveley BR, Lai
866 EC (2014) Genome-wide analysis of drosophila circular RNAs reveals their structural and
867 sequence properties and age-dependent neural accumulation. *Cell Rep* 9: 1966-1980
868 Yang M, Xiang G, Yu D, Yang G, He W, Yang S, Zhou G, Liu A (2019) Hsa_circ_0002468 Regulates
869 the Neuronal Differentiation of SH-SY5Y Cells by Modulating the MiR-561/E2F8 Axis. *Med Sci*
870 *Monit* 25: 2511-2519
871 Yang Q, Wu J, Zhao J, Xu T, Zhao Z, Song X, Han P (2018) Circular RNA expression profiles during
872 the differentiation of mouse neural stem cells. *BMC Syst Biol* 12: 128

873 You X, Vlatkovic I, Babic A, Will T, Epstein I, Tushev G, Akbalik G, Wang M, Glock C, Quedenau C
874 *et al* (2015) Neural circular RNAs are derived from synaptic genes and regulated by development
875 and plasticity. *Nat Neurosci* 18: 603-610
876 Younas N, Zafar S, Shafiq M, Noor A, Siegert A, Arora AS, Galkin A, Zafar A, Schmitz M, Stadelmann
877 C *et al* (2020) SFPQ and Tau: critical factors contributing to rapid progression of Alzheimer's
878 disease. *Acta Neuropathol* 140: 317-339
879 Zhang XO, Dong R, Zhang Y, Zhang JL, Luo Z, Zhang J, Chen LL, Yang L (2016) Diverse alternative
880 back-splicing and alternative splicing landscape of circular RNAs. *Genome Res* 26: 1277-1287
881 Zirkel A, Papantonis A (2018) Detecting Circular RNAs by RNA Fluorescence In Situ Hybridization.
882 *Methods Mol Biol* 1724: 69-75